

NANO EXPRESS

Open Access



# Dispersion-Corrected Density Functional Theory Investigations of Structural and Electronic Properties of Bulk MoS<sub>2</sub>: Effect of Uniaxial Strain

Chuong V. Nguyen<sup>1,2\*</sup> , Nguyen N. Hieu<sup>1</sup> and Duong T. Nguyen<sup>3</sup>

## Abstract

Strain-dependent structural and electronic properties of MoS<sub>2</sub> materials are investigated using first principles calculations. The structural and electronic band structures of the MoS<sub>2</sub> with relaxed unit cells are optimized and calculated by the dispersion-corrected density functional theory (DFT-D2). Calculations within the local density approximation (LDA) and GGA using PAW potentials were also performed for specific cases for the purpose of comparison. The effect of strain on the band gap and the dependence of formation energy on strain of MoS<sub>2</sub> are also studied and discussed using the DFT-D2 method. In bulk MoS<sub>2</sub>, the orbitals shift towards the higher/lower energy area when strain is applied along the z/x direction, respectively. The energy splitting of Mo4d states is in the range from 0 to 2 eV, which is due to the reduction of the electronic band gap of MoS<sub>2</sub>.

**Keywords:** Molybdenum disulphide, Uniaxial strain, Electronic property, Dispersion-corrected density functional

## Background

Molybdenum disulphide (MoS<sub>2</sub>) is an interesting material for applications in nanoelectronic applications due to its unique mechanical, electronic, and optical properties [1, 2]. It is a typical layered inorganic material, which is similar to graphite. MoS<sub>2</sub> triple layers are held together by weak van der Waals (vdW) interactions. It is a typical example of layered transition-metal dichalcogenides family, which has been studied in recent years. The MoS<sub>2</sub> attracts investigation due its distinctive industrial applications from use as a lubricant [3] and a catalyst [4] as well as in photovoltaics. By chemical bath deposition method and the mechanochemical route, MoS<sub>2</sub> films have been obtained in the experiments [5]. Due to the interlayer vdW interaction, the bulk MoS<sub>2</sub> tends to form a bilayer which is known to be an indirect semiconductor. It has indirect energy band gap of 1.23 eV [6]. The bulk MoS<sub>2</sub>

has been used in conventional industries as an intercalation agent and a dry lubricant for many years. In addition, a two-dimensional MoS<sub>2</sub> is expected for applications in nanoelectronic devices [7].

In recent years, properties of MoS<sub>2</sub> and its related structures have been theoretically studied [8–13] such as stability of structure, band gap, functionalization through adatom adsorption, and vacancy defects. By means of density functional theory computations, Chen et al. have been systematically investigated the stability and magnetic and electronic properties of MoS<sub>2</sub> nanoribbons [14, 15]. The defect structure of MoS<sub>2</sub> has also been studied [16]. Besides, the creation of magnetic and metallic characteristics in low-width MoS<sub>2</sub> nanoribbons has been studied by the first principles calculations [17]. The electronic structure of MoS<sub>2</sub> has been also studied [3]. Up to date, many works about MoS<sub>2</sub> have been done, but some questions are still worth studying. For example, the electronic properties of bulk MoS<sub>2</sub> under strain have not been enough investigated. Current studies have confirmed that the properties of low-dimensional materials

\*Correspondence: chuongnguyen11@gmail.com

<sup>1</sup> Institute of Research and Development, Duy Tan University, K7/25 Quang Trung, Da Nang, Vietnam

<sup>2</sup> School of Mechanical Engineering, Le Quy Don Technical University, Hanoi, Vietnam

Full list of author information is available at the end of the article

can be modified by strain, therefore, the response of electronic properties of bulk MoS<sub>2</sub> to the strain would be an interesting issue for discussion.

In the present work, we investigate the strain-dependent structural and electronic properties of low-dimensional MoS<sub>2</sub> materials using first principles calculations. We apply uniaxial strain onto the bulk MoS<sub>2</sub>. The structural and electronic band structures of MoS<sub>2</sub> with relaxed unit cells are optimized and calculated by the dispersion-corrected density functional theory (DFT-D2). The effects of strain on the band gap and the dependence of formation energy on strain of MoS<sub>2</sub> are also studied and discussed.

## Methods

The MoS<sub>2</sub> bulk belongs to the space group P 63/mmc. It is a layered material and a single layer consists of an S-Mo-S sandwich. In each such layer, the Mo atoms are arranged in a hexagonal lattice and are positioned in a trigonal prismatic coordination with respect to the two S layers. This implies that each Mo atom is coordinated by six S atoms. The hexagonal MoS<sub>2</sub> was selected, and the lattice parameters,  $a = 3.16 \text{ \AA}$ ,  $c/a$  ratio of 0.89 are taken as a starting point for the geometry optimization [6, 18]. Model of bulk MoS<sub>2</sub> includes two layers of S-Mo-S sandwich, which consist of one Mo atom and two S atoms in each layer, as seen in Fig. 1.

The present calculations are performed within density functional theory using accurate frozen-core full-potential projector augmented-wave (PAW) pseudopotentials [19, 20], as implemented in the Quantum

Espresso code [21]. We use the generalized gradient approximation (GGA) with the parametrization of Perdew-Burke-Ernzerhof (PBE) with added van der Waals (vdW) corrections. They are important for describing the interaction between MoS<sub>2</sub> layers. Beside DFT-D2 method, calculations within the local density approximation (LDA) and GGA using PAW potentials were also performed for specific cases. This combination is for the comparison with DFT-D2 calculations when the vdW interactions were introduced. These vdW interactions were included using the method of Grimme (DFT (PBE)-D2) [22]. This approach has been successful in describing graphene-based structures [23]. For the plane waves used in the expansion of the pseudowave functions, the cutoff energy varies in the range from 450 to 545 eV. The results of the calculations for convergence in the surface energy and interplanar distances confirmed that the cutoff energy of higher than 400 eV and the planar grid with dimensions of  $6 \times 6 \times 1$  are quite sufficient. For the different layers of the MoS<sub>2</sub>, the supercells are constructed with a vacuum space of 20 Å along the  $z$  direction. The Brillouin zones are sampled with the  $\Gamma$ -centered  $K$  point grid of  $18 \times 18 \times 1$ . The strain is simulated by setting the lattice parameter to a fixed larger value and relaxing the atomic positions. The magnitude of strain is defined as:  $\varepsilon = (a - a_0)/a_0$ , where  $a_0$  and  $a$  are the lattice parameters of the unstrained and strained systems, respectively.

The traditional density functionals are unable to give a correct description of the vdW interactions because of the dynamical correlations between fluctuating charge distributions. In the present study, we considered the

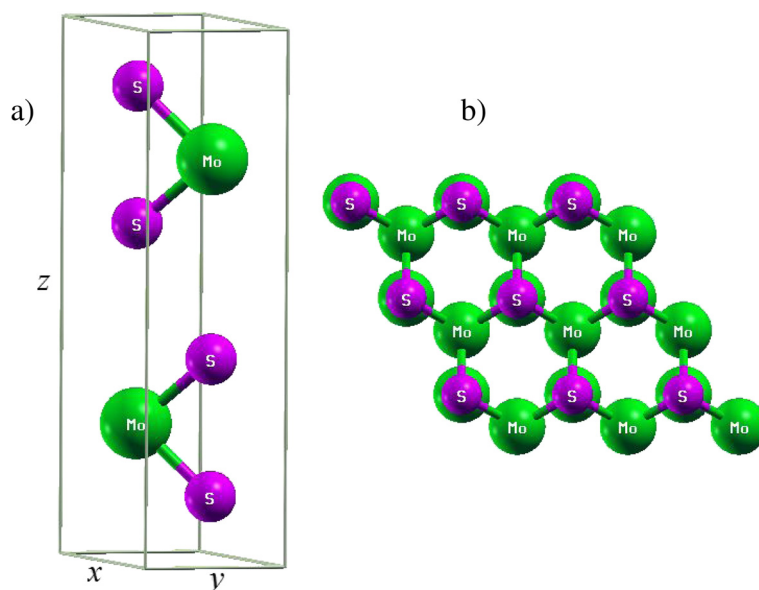


**Fig. 1** Atomic structure of the bulk MoS<sub>2</sub>. Relaxed atomic structure of the bulk MoS<sub>2</sub> from DFT-D2 calculations: **a** top view and **b** side view

vdW interaction within the DFT framework using a semi-empirical potential via the total energy functional (DFT-D2) as defined by Grimme et al. [22]. This method has been successfully applied for calculations of graphene nanoribbon/h-BN [24–26] and graphene nanoribbon/AlN [27, 28] interfaces. The total energy  $E_{\text{tot}}$  can be expressed as follows [22]:

$$E_{\text{tot}} = E_{\text{KS-DFT}} + E_{\text{disp}} = E_{\text{KS-DFT}} + E_{\text{vdW}}, \quad (1)$$

where  $E_{\text{KS-DFT}}$  is the usual self-consistent Kohn–Sham energy as obtained from the chosen DFT and  $E_{\text{disp}}$  is an empirical dispersion correction (vdW)

$$E_{\text{disp}} = -\frac{1}{2} \sum_{ij} C_{6ij} \sum_{\mathbf{R}} |\mathbf{r}_{ij} + \mathbf{R}_{ij}|^{-6} f_{\text{damp}}(|\mathbf{r}_{ij} + \mathbf{R}_{ij}|)$$

and

$$f_{\text{damp}}(|\mathbf{r}_{ij} + \mathbf{R}_{ij}|) = s_6 \left\{ 1 + \exp \left[ -d \left( \frac{|\mathbf{r}_{ij} + \mathbf{R}_{ij}|}{r_0} - 1 \right) \right] \right\}^{-1},$$

where  $\mathbf{r}_{ij} = (\mathbf{r}_j - \mathbf{r}_i)$  is the atom–atom distance vector,  $\mathbf{R} = l\mathbf{a} + m\mathbf{b} + n\mathbf{c}$  is the lattice vector,  $s_6$  is the functional-dependent scaling parameter, and  $d$  is a parameter that tunes the steepness of the damping function ( $d = 20$ ,  $s_6 = 0.75$  for PBE). The  $C_{6ij}$  coefficients are computed for each atom pair by the geometric mean of atomic terms  $C_{6ij} = \sqrt{C_{6i}C_{6j}}$ , and the  $r_0$  term is computed by the simple sum of vdW radii of the atom pairs  $r_0 = r_{0i} + r_{0j}$ .

## Results and Discussion

### Structural and Electronic Properties of the Bulk MoS<sub>2</sub>

Our calculations for the geometrical parameters and band gap of the bulk MoS<sub>2</sub> using different methods are listed in Table 1. By using three different methods, our calculations show that the lattice parameter  $a$  for the bulk MoS<sub>2</sub> is 3.116, 3.172, and 3.176 Å corresponding to the LDA, GGA, and DFT-D2 methods, respectively. This result is in good agreement with other theoretical [29, 30] and experimental [6, 18] studies, as shown in Table 1.

**Table 1** Calculated structural parameters and band gap of the bulk MoS<sub>2</sub> using LDA, GGA, and DFT-D2 methods

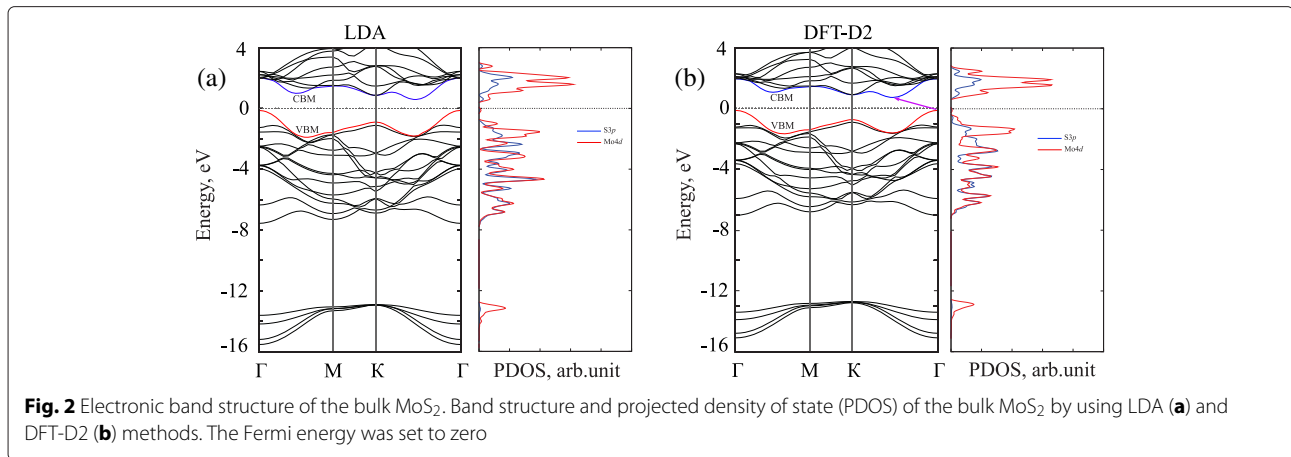
	Lattice constant		$E_g$ , eV	$d_{\text{Mo-S}}$ , eV
	$a$ , Å	$c/a$		
LDA	3.115	3.85	0.72	2.36
GGA	3.172	3.95	0.96	2.43
DFT-D2	3.176	3.85	1.22	2.41
Theory (LDA)	3.13 [29]	3.84 [29]	0.75 [29]	2.39 [29]
	3.11 [30]	-	0.72 [30]	2.37 [30]
Theory (GGA)	3.23 [29]	4.01 [29]	1.05 [29]	2.45 [29]
	3.20 [30]	-	0.85 [30]	2.42 [30]
Experiment	3.16 [18]	3.89 [18]	1.23 [6]	2.41 [18]

We calculate the electronic band gap of the bulk MoS<sub>2</sub> by using different methods (LDA, GGA, and DFT-D2). We see that the band gap value calculated by the LDA and GGA methods is smaller than that of the experimental study. Our result for the band gap of the bulk MoS<sub>2</sub> form is 0.72 eV (0.96 eV) using LDA (GGA) functionals, which is in good agreement with the available theoretical data of 0.72 eV (0.85 eV) using the same LDA-PAW (GGA) functionals [30, 31]. These values are smaller than that of the experimental study (1.23 eV) [6]. This difference is due to the inherent drawback of standard LDA/GGA functionals. However, the DFT-D2 calculations for the band gap give results (1.20 eV) that are in good agreement with the experimental data (1.23 eV) [6]. Besides, our DFT-D2 calculations give the bond length  $d_{\text{Mo-S}}$  being 1.41 Å. That is the same value as in the experimental study. The match between the DFT-D2 method and the experimental study can be explained by the existence of the vdW interaction in MoS<sub>2</sub>. Our DFT-D2 calculations is including the vdW interaction. We believe that the DFT-D2 method is a suitable method for the structural and electronic properties of the bulk MoS<sub>2</sub>.

Figure 2 shows the projected density of state (PDOS) of the ideal bulk MoS<sub>2</sub> form. It shows that the valence band consists of two main bands, in which the lower band (from -14.0 eV to -13.0 eV) below the Fermi level  $E_F$  ( $E_F = 0$ ) is mainly due to S3s states. Upper valence bands (from -7.0 eV to -0.5 eV) involve the noticeable contributions of the Mo4d and S3p states. This results in hybridized Mo4d-S3p interactions and provides the covalent component of the Mo-S bonds in bulk MoS<sub>2</sub>. Besides, the lower edge of the conduction band of the bulk MoS<sub>2</sub> involves mainly the antibonding Mo4d states. The bands around the energy band gap are relatively flat, as expected from the  $d$  character of the electron states at these energies. Our DFT-D2 band structure calculations show that the bulk MoS<sub>2</sub> has an indirect band gap of 1.22 eV opening between the lowest energy of the conduction band (located at between the  $\Gamma$  and  $K$  points) and the highest energy of the valence band (located at the  $\Gamma$  point) (see Fig. 2).

### Effect of Uniaxial Strain on the Structural and Electronic Properties of MoS<sub>2</sub>

In this part, we consider the influence of uniaxial strain on the structural and electronic properties of the bulk MoS<sub>2</sub>. Uniaxial strain along both  $x$  and  $z$  directions is considered in our study (see, Fig. 1). The components of strain along the  $x$  and  $z$  directions are noted as  $\varepsilon_x$  and  $\varepsilon_z$ , respectively. The strains are evaluated as the lattice stretching percentage. We defined  $\varepsilon_x = (a - a_0)/a_0$  and  $\varepsilon_z = (c - c_0)/c_0$ , where  $a_0$  and  $c_0$  are the lattice constants at the equilibrium state, and  $a$  and  $c$  are strained lattice constants. A wide range of strain along (up to 10 %) both directions



with step  $\Delta\varepsilon = 2\%$  has been employed in the present study.

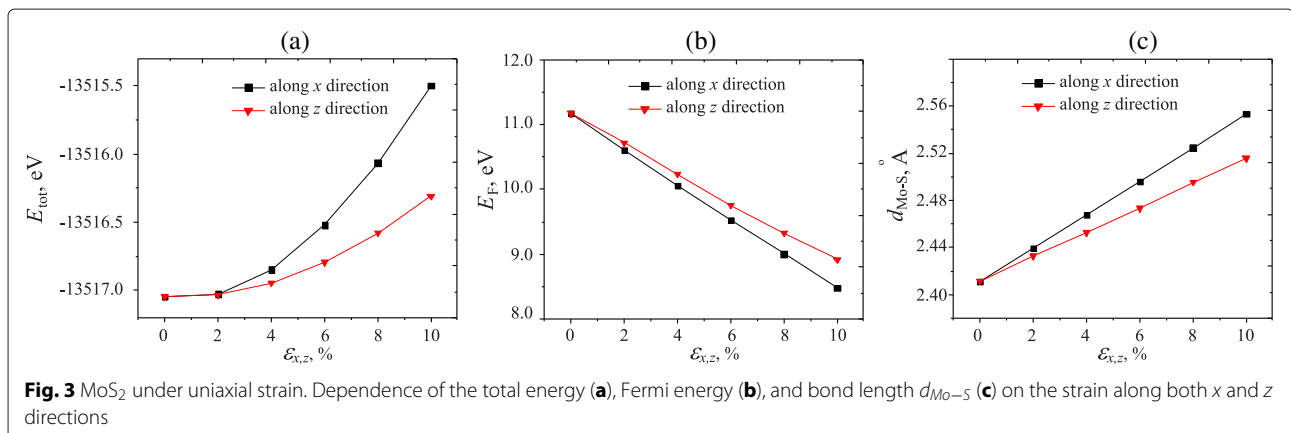
Figure 3 shows the dependence of the total energy, the Fermi energy  $E_F$ , and bond length  $d_{Mo-S}$  on the strain. At the equilibrium state (unstrained), the total energy of the bulk MoS<sub>2</sub> is minimum. The dependence of total energy on uniaxial strain can be described by a hyperbolic shape as shown in Fig. 3a. Figure 3a also shows that the total energy of bulk MoS<sub>2</sub> along the  $x$  direction is higher than that along the  $z$  direction. When the strain along the  $x$  direction is applied, the bulk MoS<sub>2</sub> turns out to be less stable than that of the strain along the  $z$  direction.

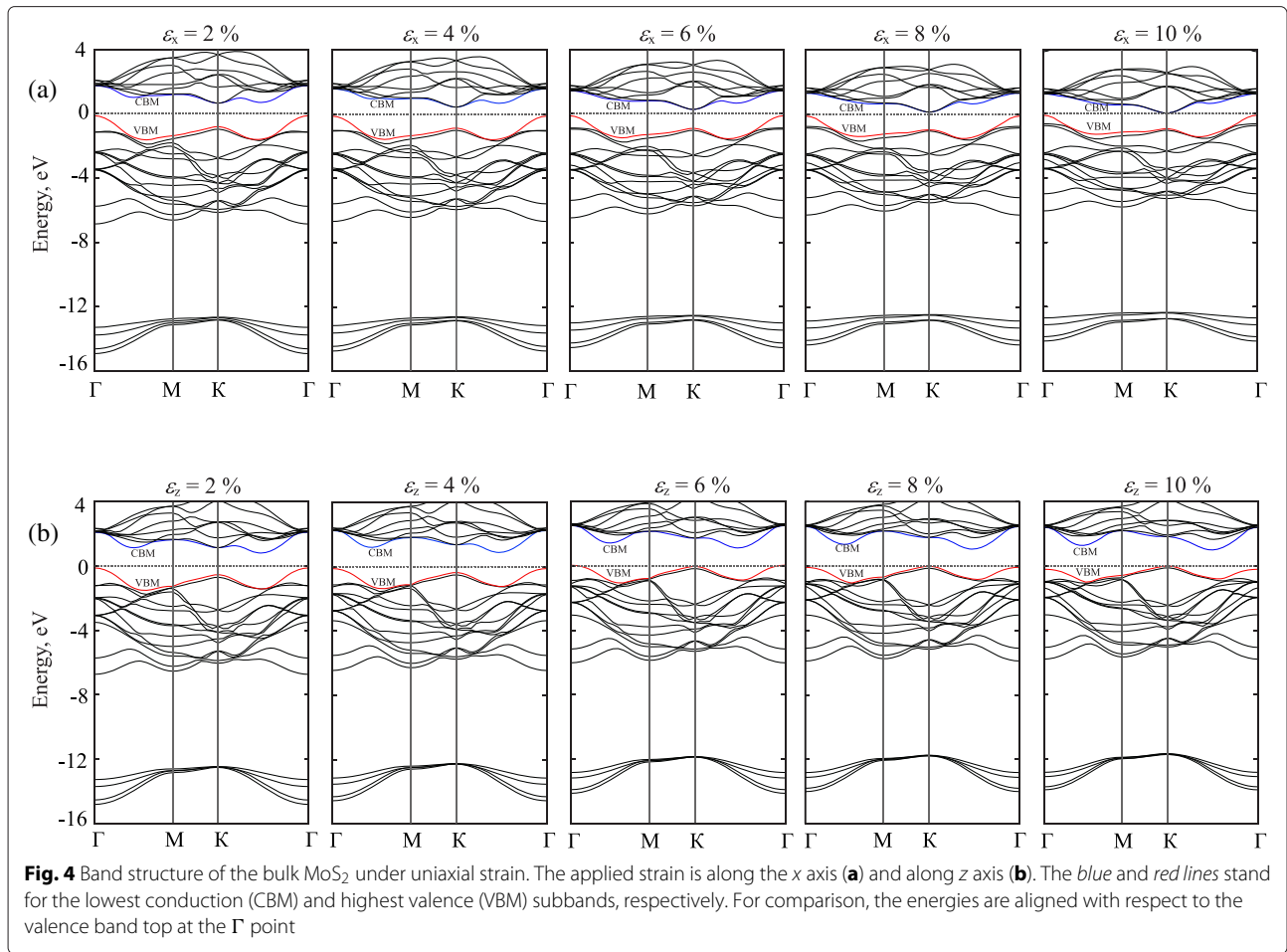
Figure 3b, c shows the dependence of Fermi level  $E_F$  and bond length  $d_{Mo-S}$  in the bulk MoS<sub>2</sub> on the strain along  $x$  and  $z$  directions. Under uniaxial strain, the Fermi energy and the Mo-S bond length change linearly with strain. As the uniaxial strain increases, the Fermi energy is decreased and the bond length  $d_{Mo-S}$  increases. We can see that the total energy, Fermi energy, and bond length depend not only on strain strength but also depend strongly on the direction of the applied strain.

The effect of the uniaxial strain on the electronic band structure and energy band gap of bulk MoS<sub>2</sub> is shown in

Figs. 4 and 5, respectively. Both  $x$  and  $z$  directions of strain are taken into account. We can see that the electronic properties of bulk MoS<sub>2</sub> are sensitive to the uniaxial strain. The band gap strongly depends not only on the elongation but also on the strain direction (see, Fig. 5). As shown in Fig. 4, we can see that in the bulk MoS<sub>2</sub>, the orbitals will be shifted towards a higher/lower energy level at the  $K$  point when strain is applied along the  $z/x$  direction, respectively. The states at top of the valence band and bottom of the conduction band near the  $\Gamma$  point, which originate mainly from  $d$  orbitals on Mo atoms and contributions of  $p_z$  orbitals on S atoms, are accordingly independent on the uniaxial strain. When  $\varepsilon_x$  strain is applied, we observe a shift of orbitals in the conduction bands towards the lower energy region, while all orbitals of valence bands shift toward the Fermi level, which is in result of a reduction of the band gap energy. Similarly, when  $\varepsilon_z$  strain is applied, the shift of orbitals are also observed but in the valence band. It shifts towards the higher energy region.

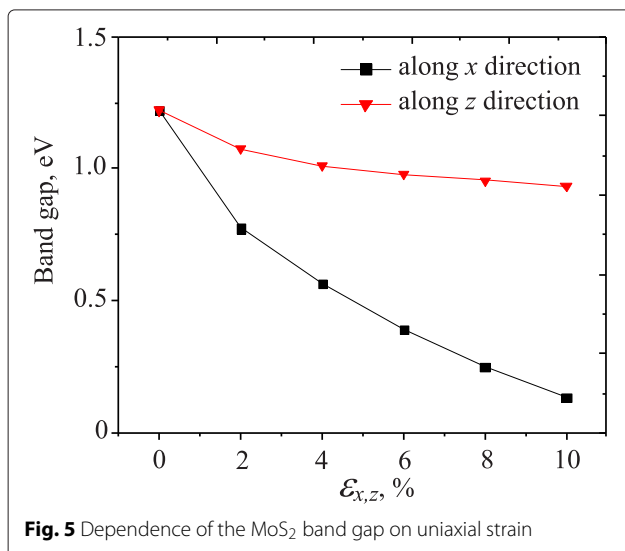
At equilibrium, the lowest energy of the conduction band ( $E_K^{CBM}$ ) and the highest energy of the valence band ( $E_K^{VBM}$ ) are 0.903 and  $-0.736$  eV, respectively. These values of energy are decreased due to increasing the strain





strength. Especially, when the strain increases from 0 to 10 %,  $E_K^{CBM}$  decreases from 0.903 to 0.08 eV.

Figure 5 depicts the energy band gap as a function of the applied  $\epsilon_{xz}$  strain. Under  $\epsilon_x$  strain, the band gap decreases monotonically with strain. We can see that at  $\epsilon_x = 2\%$ ,



the band gap is equal to 0.78 eV. This band gap decreases to 0.13 eV when  $\epsilon_x = 10\%$ . The effect of the  $\epsilon_z$  on the band gap of the MoS<sub>2</sub> is negligible (in comparison to the case of strain applied along the *x* direction). We see that when the  $\epsilon_z < 6\%$ , the point in *k*-space corresponding to the highest energy of the valence band is located at the  $\Gamma$  point and it will be shifted to the *K* point in the first Brillouin zone when the  $\epsilon_z > 6\%$ . The band gap of the bulk MoS<sub>2</sub> is strongly dependent on the applied strain along the *x* direction and we expect that a phase transition will occur in the case of larger deformation.

In addition, we also calculate band gap of bulk MoS<sub>2</sub> under uniaxial strain along the armchair direction (*y* direction). Similar to the case of strain along the zigzag direction, band gap of MoS<sub>2</sub> reduces concurrently with strain. Our calculations show that the change in band gap of MoS<sub>2</sub> under uniaxial strain along the zigzag and armchair directions is almost the same. This result is in good agreement with the previous works [32, 33].

The strain dependence of the projected density of states (PDOS) of the Mo4*d* and S3*p* states is shown in Fig. 6. It shows that, under the uniaxial strain, an energy splitting of

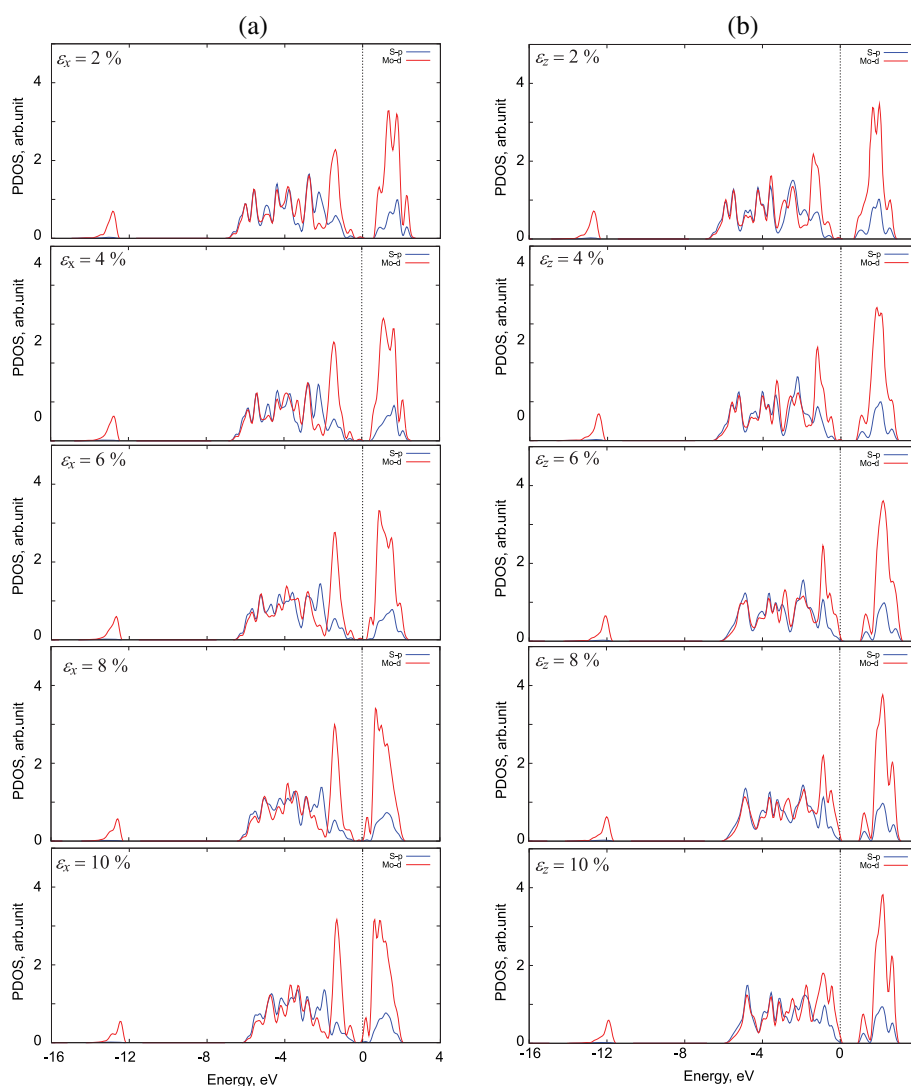


**Fig. 6** The PDOS of the Mo4d and S3p states under strain. The PDOS of the Mo4d and S3p states of the bulk MoS<sub>2</sub> form under applied  $\epsilon_x$  **(a)** and  $\epsilon_z$  **(b)** strain, respectively

Mo4d states in the range from 0 to 2 eV is observed. The effect may be associated with crystal field theory, in which the loss of degeneracy of Mo4d orbitals in transition metal complexes is described. The energy splitting of the Mo4d orbitals is observed in both cases of strain, as shown in

Fig. 6. Figure 7 shows the isosurface of lowest unoccupied crystal orbitals at the K point in the first Brillouin zone of the bulk MoS<sub>2</sub> in the case of with and without strain. Based on the partial charge density distribution, we see that the change in electronic properties of the bulk MoS<sub>2</sub>

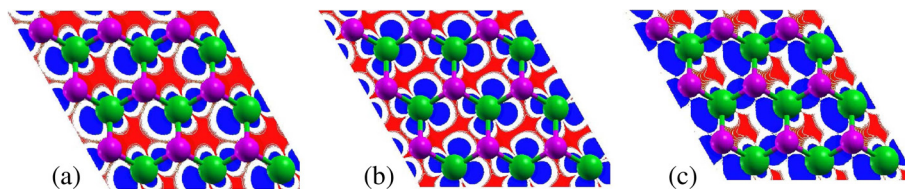


**Fig. 7** Isosurfaces of lowest unoccupied crystal orbitals (CBM) at the K point in the first Brillouin zone of the bulk MoS<sub>2</sub> under the applied strain. **a**  $\epsilon_{xz} = 0$ , **b**  $\epsilon_x = 8\%$ , **c**  $\epsilon_z = 8\%$

is determined by the strength of the Mo-S bond. Figure 7 also shows that the lowest energy of the conduction band at *K* point is mainly contributed by the coupling between the *Mo4d* and *S3p* orbitals.

## Conclusions

In this paper, we studied the effect of uniaxial strain on the structural and electronic properties of the bulk MoS<sub>2</sub> using first principles calculations. Methodologically, we pointed out that the DFT-D2 calculations are a suitable method for calculations of structural and electronic properties of the bulk MoS<sub>2</sub>. Our calculations showed that the electronic properties of the bulk MoS<sub>2</sub> are very sensitive to the uniaxial strain, especially when the strain is applied along the *x* direction. The band gap of the bulk MoS<sub>2</sub> decreases linearly with an increase of the strain strength and we can control the energy splitting and band gap of the bulk MoS<sub>2</sub> by the strain. This makes MoS<sub>2</sub> becoming a promising material for application in nanoelectronic device such as nanosensors.

## Competing Interests

The authors declare that they have no competing interests.

## Authors' Contributions

CVN, NNH, and DTN carried out the simulations. CVN and NNH participated in the design of the study, performed the data analysis, and wrote the manuscript. All authors read and approved the final manuscript.

## Author details

<sup>1</sup>Institute of Research and Development, Duy Tan University, K7/25 Quang Trung, Da Nang, Vietnam. <sup>2</sup>School of Mechanical Engineering, Le Quy Don Technical University, Hanoi, Vietnam. <sup>3</sup>School of Engineering Physics, Hanoi University of Science and Technology, Hanoi, Vietnam.

Received: 23 August 2015 Accepted: 28 September 2015

Published online: 04 November 2015

## References

- Chhowalla M, Shin HS, Eda G, Li L-J, Loh KP, Zhang H (2013) The chemistry of two-dimensional layered transition metal dichalcogenide nanosheets. *Nat Chem* 5(4):263–275. doi:10.1038/nchem.1589
- van der Zande AM, Huang PY, Chenet DA, Berkelbach TC, You Y, Lee G-H, Heinz TF, Reichman DR, Muller DA, Hone JC (2013) Grains and grain boundaries in highly crystalline monolayer molybdenum disulphide. *Nat Mater* 12(6):554–561. doi:10.1038/nmat3633
- Lebegue S, Eriksson O (2009) Electronic structure of two-dimensional crystals from ab initio theory. *Phys Rev B* 79(11):115409. doi:10.1103/PhysRevB.79.115409
- Hu KH, Hu XG, Sun XJ (2010) Morphological effect of MoS<sub>2</sub> nanoparticles on catalytic oxidation and vacuum lubrication. *Appl Surf Sci* 256(8):2517–2523. doi:10.1016/j.apsusc.2009.10.098
- Garadkar K, Patil A, Hankare P, Chate P, Sathe D, Delekar S (2009) MoS<sub>2</sub>: preparation and their characterization. *J Alloys Compd* 487(1):786–789. doi:10.1016/j.jallcom.2009.08.069
- Mak KF, Lee C, Hone J, Shan J, Heinz TF (2010) Atomically thin MoS<sub>2</sub>: a new direct-gap semiconductor. *Phys Rev Lett* 105(13):136805. doi:10.1103/PhysRevLett.105.136805
- Tang Q, Zhou Z (2013) Graphene-analogous low-dimensional materials. *Prog Mater Sci* 58(8):1244–1315
- Xu W-B, Huang B-J, Li P, Li F, Zhang C-W, Wang P-J (2014) The electronic structure and optical properties of mn and b, c, n co-doped MoS<sub>2</sub> monolayers. *Nanoscale Res Lett* 9(1):554. doi:10.1186/1556-276X-9-554
- Yue Q, Shao Z, Chang S, Li J (2013) Adsorption of gas molecules on monolayer MoS<sub>2</sub> and effect of applied electric field. *Nanoscale Res Lett* 8(1):425. doi:10.1186/1556-276X-8-425
- Li X, Wu S, Zhou S, Zhu Z (2014) Structural and electronic properties of germanene/MoS<sub>2</sub> monolayer and silicene/MoS<sub>2</sub> monolayer superlattices. *Nanoscale Res Lett* 9(1):110. doi:10.1186/1556-276X-9-110
- Lu S-C, Leburton J-P (2014) Electronic structures of defects and magnetic impurities in MoS<sub>2</sub> monolayers. *Nanoscale Res Lett* 9(1):676. doi:10.1186/1556-276X-9-676
- Jing Y, Tan X, Zhou Z, Shen P (2014) Tuning electronic and optical properties of MoS<sub>2</sub> monolayer via molecular charge transfer. *J Mater Chem A* 2(40):16892–16897
- Tang Q, Zhou Z, Chen Z (2015) Innovation and discovery of graphene-like materials via density-functional theory computations. *Wiley Interdiscip Rev Clim Chang Comput Mol Sci* 5(5):360–379
- Li Y, Zhou Z, Zhang S, Chen Z (2008) MoS<sub>2</sub> nanoribbons: high stability and unusual electronic and magnetic properties. *J Am Chem Soc* 130(49):16739–16744
- Li Y, Wu D, Zhou Z, Cabrera CR, Chen Z (2012) Enhanced Li adsorption and diffusion on MoS<sub>2</sub> zigzag nanoribbons by edge effects: a computational study. *J Phys Chem Lett* 3(16):2221–2227
- Spirko JA, Neiman ML, Oelker AM, Klier K (2003) Electronic structure and reactivity of defect MoS<sub>2</sub>: I. relative stabilities of clusters and edges, and electronic surface states. *Surf Sci* 542(3):192–204. doi:10.1016/S0039-6028(03)00957-9
- Shidpour R, Manteghian M (2009) The creation of the magnetic and metallic characteristics in low-width MoS<sub>2</sub> nanoribbon (1d MoS<sub>2</sub>): A [DFT] study. *Chem Phys* 360(1–3):97–105. doi:10.1016/j.chemphys.2009.04.015
- Wilson J, Yoffe A (1969) The transition metal dichalcogenides discussion and interpretation of the observed optical, electrical and structural properties. *Adv Phys* 18(73):193–335. doi:10.1080/00018736900101307
- Blöchl PE (1994) Projector augmented-wave method. *Phys Rev B* 50(24):17953. doi:10.1103/PhysRevB.50.17953
- Kresse G, Joubert D (1999) From ultrasoft pseudopotentials to the projector augmented-wave method. *Phys Rev B* 59(3):1758. doi:10.1103/PhysRevB.59.1758
- Giannozzi P, Baroni S, Bonini N, Calandra M, Car R, Cavazzoni C, Ceresoli D, Chiarotti GL, Cococcioni M, Dabo I, Corso AD, de Gironcoli S, Fabris S, Fratesi G, Gebauer R, Gerstmann U, Gougousis C, Kokalj A, Lazzeri M, Martin-Samos L, Marzari N, Mauri F, Mazzarello R, Paolini S, Pasquarello A, Paulatto L, Sbraccia C, Scandolo S, Sclauzero G, Seitsonen AP, Smogunov A, Umari P, Wentzcovitch RM (2009) Quantum espresso: a modular and open-source software project for quantum simulations of materials. *J Phys Condens Matter* 21(39):395502. doi:10.1088/0953-8984/21/39/395502
- Grimme S (2004) Accurate description of van der Waals complexes by density functional theory including empirical corrections. *J comput chem* 25(12):1463–1473. doi:10.1002/jcc.20078
- Nguyen CV, Ilyasov VV, Nguyen HN (2015) Tuning the electronic properties of armchair graphene nanoribbons by strain engineering. *Phys Scr* 90(1):015802. doi:10.1088/0031-8949/90/1/015802
- Ilyasov VV, Meshi BC, Nguyen VC, Ershov IV, Nguyen DC (2014) Magnetism and transport properties of zigzag graphene nanoribbons/hexagonal boron nitride heterostructures. *J Appl Phys* 115(5). doi:10.1063/1.4864261
- Ilyasov VV, Nguyen CV, Ershov IV, Nguyen CD, Hieu NN (2015) Modulation of the band structure in bilayer zigzag graphene nanoribbons on hexagonal boron nitride using the force and electric fields. *Mater Chem Phys* 154:78–83. doi:10.1016/j.matchemphys.2015.01.047
- Ilyasov VV, Meshi BC, Nguyen VC, Ershov IV, Nguyen DC (2014) Tuning the band structure, magnetic and transport properties of the zigzag graphene nanoribbons/hexagonal boron nitride heterostructures by transverse electric field. *J Chem Phys* 141(1). doi:10.1063/1.4885857
- Ilyasov VV, Nguyen CV, Ershov IV, Hieu NN (2015) Electric field and substrate-induced modulation of spin-polarized transport in graphene nanoribbons on a3b5 semiconductors. *J Appl Phys* 117(17). doi:10.1063/1.4919920
- Ilyasov VV, Nguyen CV, Ershov IV, Hieu NN (2015) Effect of electric field on the electronic and magnetic properties of a graphene nanoribbon/aluminium nitride bilayer system. *RSC Adv* 5:49308–49316. doi:10.1039/C5RA06239J

29. Kumar A, Ahluwalia P (2012) A first principle comparative study of electronic and optical properties of 1H-MoS<sub>2</sub> and 2H-MoS<sub>2</sub>. *Mater Chem Phys* 135(2):755–761. doi:10.1016/j.matchemphys.2012.05.055
30. Ataca C, Ciraci S (2011) Functionalization of single-layer MoS<sub>2</sub> honeycomb structures. *J Phys Chem C* 115(27):13303–13311. doi:10.1021/jp2000442
31. Ataca C, Sahin H, Aktürk E, Ciraci S (2011) Mechanical and electronic properties of MoS<sub>2</sub> nanoribbons and their defects. *J Phys Chem C* 115(10):3934–3941. doi:10.1021/jp1115146
32. Johari P, Shenoy VB (2012) Tuning the electronic properties of semiconducting transition metal dichalcogenides by applying mechanical strains. *ACS Nano* 6(6):5449–5456. doi:10.1021/nn301320r
33. Lu P, Wu X, Guo W, Zeng XC (2012) Strain-dependent electronic and magnetic properties of MoS<sub>2</sub> monolayer, bilayer, nanoribbons and nanotubes. *Phys Chem Chem Phys* 14(37):13035–13040

**Submit your manuscript to a SpringerOpen<sup>®</sup> journal and benefit from:**

- Convenient online submission
- Rigorous peer review
- Immediate publication on acceptance
- Open access: articles freely available online
- High visibility within the field
- Retaining the copyright to your article

---

Submit your next manuscript at ► [springeropen.com](http://springeropen.com)

---